NSEL Report Series
Report No. NSEL-021
February 2010

Characterization of Wireless Smart Sensor Performance

Lauren E. Linderman
Jennifer A. Rice
Suhail Barot
Billie F. Spencer, Jr.
Jennifer T. Bernhard

NSEL
NEWMARK STRUCTURAL ENGINEERING LABORATORY

Department of Civil and Environmental Engineering
University of Illinois at Urbana-Champaign

UILU-ENG-2010-1801

ISSN: 1940-9826

The Newmark Structural Engineering Laboratory (NSEL) of the Department of Civil and Environmental Engineering at the University of Illinois at Urbana-Champaign has a long history of excellence in research and education that has contributed greatly to the state-of-the-art in civil engineering. Completed in 1967 and extended in 1971, the structural testing area of the laboratory has a versatile strong-floor/wall and a three-story clear height that can be used to carry out a wide range of tests of building materials, models, and structural systems. The laboratory is named for Dr. Nathan M. Newmark, an internationally known educator and engineer, who was the Head of the Department of Civil Engineering at the University of Illinois [1956-73] and the Chair of the Digital Computing Laboratory [1947-57]. He developed simple, yet powerful and widely used, methods for analyzing complex structures and assemblages subjected to a variety of static, dynamic, blast, and earthquake loadings. Dr. Newmark received numerous honors and awards for his achievements, including the prestigious National Medal of Science awarded in 1968 by President Lyndon B. Johnson. He was also one of the founding members of the National Academy of Engineering.

Contact:
Prof. B.F. Spencer, Jr.
Director, Newmark Structural Engineering Laboratory
2213 NCEL, MC-250
205 North Mathews Ave.
Urbana, IL 61801
Telephone (217) 333-8630
E-mail: bfs@illinois.edu

This paper is an expanded version of the paper under the same title that is scheduled to appear in the ASCE Journal of Engineering Mechanics. The authors gratefully acknowledge the support of this research by the National Science Foundation, under grant CMS 06-00433 (Dr. S. C. Liu, program manager) and the use of the anechoic test-bed supported by NSF grant CNS 04-23431. The authors would like to thank Kirill Mechitov for his invaluable knowledge of the Imote2 and development of the TestRadio communication evaluation software tool.

The cover photographs are used with permission. The Trans-Alaska Pipeline photograph was provided by Terra Galleria Photography (http://www.terragalleria.com/).

ABSTRACT

A critical aspect of using wireless sensors for structural health monitoring is communication performance. Unlike wired systems, data transfer is less reliable between wireless sensor nodes due to data loss. While reliable communication protocols are typically used to reduce data loss, this increase in communication can drain already limited power resources. This report provides an experimental investigation of the wireless communication characteristics of the Imote2 smart sensor platform; the presentation is tailored towards the end user, e.g., application engineers and researchers. Following a qualitative discussion of wireless communication and packet delivery, a quantitative characterization of wireless communication capabilities of the Imote2 platform is provided, including an assessment of onboard and external antenna performance. Herein, the external antenna was found to significantly outperform the onboard antenna in both transmission and reception reliability. However, the built environment, including building materials and other wireless networks, can significantly reduce reception rate and thus increase packet loss. Finally, implications of these results for a full-scale implementation are presented.

CONTENTS

Chapter 1

INTRODUCTION

As civil infrastructure ages, the ability to monitor structural health is becoming essential. The recent I-35 bridge collapse in Minnesota highlights the need for structural health monitoring and damage detection so such events can be avoided. Damage is a highly local phenomenon and thus is expected to require a dense array of sensors to achieve adequate monitoring performance. Current installation costs for wired sensors are high, making realization of a dense network prohibitively expensive. Alternatively, the use of wireless smart sensors, which include onboard computation and memory, has the potential to significantly reduce implementation costs (Spencer et al. 2004), thus facilitating deployment of a dense network of sensors for structural health monitoring (Nagayama and Spencer 2007).

However, due to the limited power and communication resources of smart sensors, several challenges are associated with their use for large-scale structural monitoring. This report focuses on the key issue that, unlike wired systems, data transfer between wireless sensor nodes is intrinsically unreliable due to channel impairments between the transmitter and receiver. Data loss due to channel impairments can significantly degrade otherwise good quality sensor data and result in inaccurate estimates of the state of a structure's health (Nagayama et al. 2007).

Thus far, reliable wireless communication protocols have often been used to reduce these effects (Nagayama and Spencer 2007) and some research has been conducted toward understanding the impact of lossy wireless communication (Nagayama and Spencer 2007; Nagayama et al. 2007; Pei et al. 2007). In near real-time monitoring systems, reliable communication protocols that consist of multiple acknowledgments and resending of data are used to prevent data loss (Nagayama and Spencer 2007). However, given that communication can be power intensive, this increase in communication can more quickly deplete already limited network resources.

The reliability of wireless communication is influenced by characteristics such as communication range, physical interference, multi-path effects, and noise, all of which contribute to data loss (Shankar 2002, Grimmer and Suh 2005). Significant work has been done to understand these issues in wireless data transmission; for example Zhao and Govindan (2003), Seidel and Rappoport (1992), and Lee and Chanson (2002) all discuss data propagation and loss in wireless systems. In addition, wireless communication channels and protocols themselves have been studied by Hyas and Radha (2008). Pei et al. (2007) explored the influence of environmental factors on reliable real-time wireless communication and more specifically the distribution of lost data within a measurement record. However, limited experimental characterization of the wireless communication hardware used by smart sensing platforms used in SHM applications has been reported to date.

This report examines experimentally the capabilities and limitations of smart sensor wireless communication hardware with a focus on SHM applications. Chapter 2 gives an overview of the smart sensing platform used in the study and a qualitative description of wireless communication and packet delivery. The Imote2 smart sensing platform is

uniquely capable to meet the data intensive requirements of SHM applications (Spencer et al. 2008) and is thus chosen for this investigation. Chapter 3 provides a quantitative characterization of the wireless communication capabilities of the Imote2 platform, including an assessment of both onboard and external antenna performance. The ideal communication performance is investigated along with the impact of the built environment on wireless communication. Subsequently, in Chapter 4, the impact of external antenna performance is discussed with respect to full-scale implementation, including the results of tests conducted on a historic steel truss bridge.

OVERVIEW OF COMPONENTS AND WIRELESS COMMUNICATION

In this section, a qualitative understanding of wireless sensor communication is provided, including an overview of the key components of the wireless sensor used in this study, and a discussion of how the software enables wireless communication.

2.1 Wireless Smart Sensor Platform

While a number of smart sensor platforms are commercially available (Lynch and Loh 2006), this research utilizes the Imote2 as it possesses the features required for the demands of data intensive applications such as SHM. The Imote2, pictured in Fig. 2.1, has a low-power X-scale processor (PXA27x) with user selectable processor speed to optimize power consumption. The available memory includes 256 KB of integrated RAM, 32 MB of external SDRAM, and 32 MB of flash memory. The elements of the platform associated with wireless communication are described briefly.

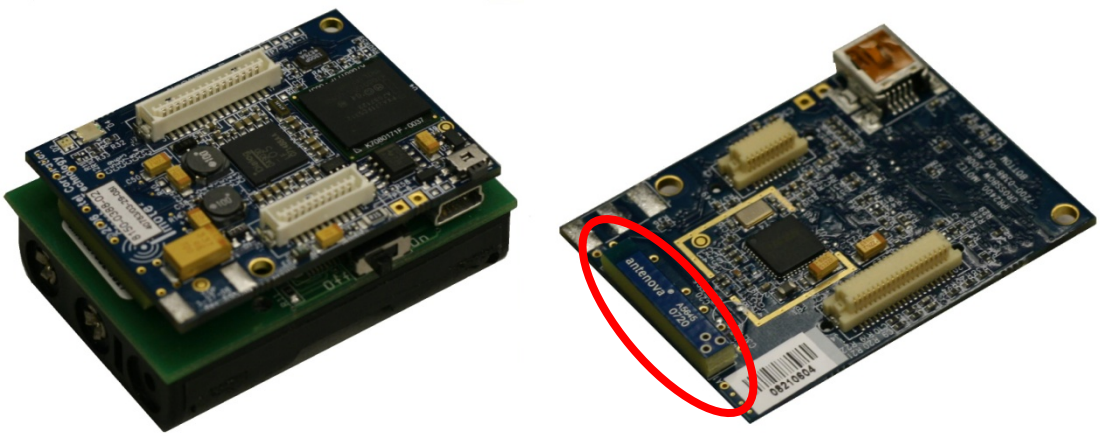

Figure 2.1: Imote2 with battery board (left) and bottom view of processor board with onboard antenna (right).

Radio

The radio chip used on the Imote2 is the Chipcon CC2420 2.4 GHz IEEE 802.15.4 RF transmitter. The popular radio chip is also used on the MicaZ, Mica2 and Telos smart sensor platforms (Lynch and Loh 2006). The chip is a byte-level radio ideal for low-voltage, low-power wireless applications (Chipcon 2004). The radio supports multiple transmission options that can be tailored to the application to optimize network performance. As part of this study, the effects of varying two of the primary transmission options are studied: (1) transmission channel (or frequency) and (2) transmission power. The selection of the appropriate transmission frequency is important when other wireless devices operating in the 2.4 GHz frequency band are within range of the sensor network. Appropriate transmission channel selection will be discussed in more detail in a

subsequent section. The selection of the optimal transmission power is critical for power and network management. Higher transmission power allows the sensors to achieve longer communication distances but results in higher current consumption on the sensor node. Limiting the current consumption will reduce the amount of battery power consumed by RF communication over the life of the network. Moreover, limiting communication range can reduce packet collisions when multiple sensors communicate simultaneously.

The CC2420 transmission power output ranges from -25 dBm to 0 dBm; the corresponding power level and current consumption are shown in Table 2.1. In receiver mode, the typical current consumption is 19.7 mA.

Table 2.1: Output power options and corresponding current consumption (Chipcon 2004).

Power Command	Output Power (dBm)	Current Consumption (mA)
31	0	17.4
27	-1	16.5
23	-3	15.2
19	-5	13.9
15	-7	12.5
11	-10	11.2
7	-15	9.9
3	-25	8.5

Antenna

The Imote2's onboard antenna is the Antenova Mica 2.4 GHz SMD pictured in Fig. 2.1. The onboard antenna is designed to use the printed circuit board on which it is mounted as a ground plane (Antenova 2007a); thus, the antenna's placement on the board greatly affects its performance. The antenna offers a peak gain of 1.8 dBi.

An optional external antenna may also be used in conjunction with the Imote2. For this study, the Antenova Titanis 2.4 GHz Swivel SMA antenna is chosen (see Fig. 2.2). The antenna is 4.83 cm in length which gives it an electrical size of ~0.4λ, where λ is wavelength at the operating frequency. The antenna has a peak gain of 2.2 dBi. One advantage of this antenna is that the blade can rotate 360°, thus allowing optimal antenna orientation (Antenova 2007b). A more thorough discussion of both internal and external antenna behavior will be given later.

Figure 2.2: Imote2 with battery board and external antenna.

Operating System

As with many wireless sensor platforms, the Imote2 employs TinyOS as its operating system. TinyOS is tailored to the specific constraints of wireless sensor network applications. In particular, it has a small memory footprint while efficiently supporting complex application programs (Levis et al. 2005).

2.2 Software Considerations in Wireless Communication

Unlike in wired sensor systems, where data is transmitted solely via hardware, wireless sensor data transmission requires the interaction of the software and radio hardware. Fig. 2.3 depicts a simplified framework for wireless communication that illustrates how these two elements interact (Buonadonna 2002). Within this framework, several concepts unique to wireless communication, including the radio packet and packet error detection, are addressed. While this communication scheme is common, the details will depend on the specific hardware, software, and application.

Within the software application, the data to be communicated and its routing information are placed in packets and sent wirelessly over the network. A *packet* consists of four parts: preamble, header, data and footer. The portions of the packet formed by the application are the header, which contains the routing and packet information, and the data. This study considers only a fixed payload scheme where the number of bytes in a packet issued by the application does not change. Here, a fixed packet size of 28 bytes, which is the TinyOS default, is chosen, consisting of 4 bytes for the header and 24 bytes for the data. This packet is then sent to the radio driver in TinyOS. Because data sets can be large, numerous packets are typically transmitted by the application.

Prior to transmission, the radio driver adds a preamble and footer to each packet. The footer includes the cyclic redundancy check (CRC), which characterizes the packet and is used for error detection after transmission. The radio packet is then separated and transmitted in a byte-by-byte manner by the radio.

Similarly, in receiving mode, the radio hardware receives the transmitted data byte-by-byte, which the radio driver then assembles into the radio packet based on the preamble. . The preamble signals the start of the radio packet and synchronizes the transmitter and receiver. Upon successful packet reception, the driver within TinyOS then

processes the packet to determine whether it should be retained or dropped. The CRC is used for this error detection. If the CRC does not correspond with the received packet then an error has occurred. If the packet is retained, it is then available to the application.

Two primary packet error types can occur. In the first, if a single bit gets flipped (e.g., a '0' to a '1' or vice versa) during transmission, the radio chip can correct the error. For the second error type, multiple bit errors are present in the received packet. If multiple bits within the preamble are corrupted, the driver does not recognize the start of the packet and ignores the entire packet. If the bit errors are within the packet, the CRC check fails and the entire packet is dropped. In other words, a single bit error can be fixed, while multiple bit errors cause the packet to be dropped.

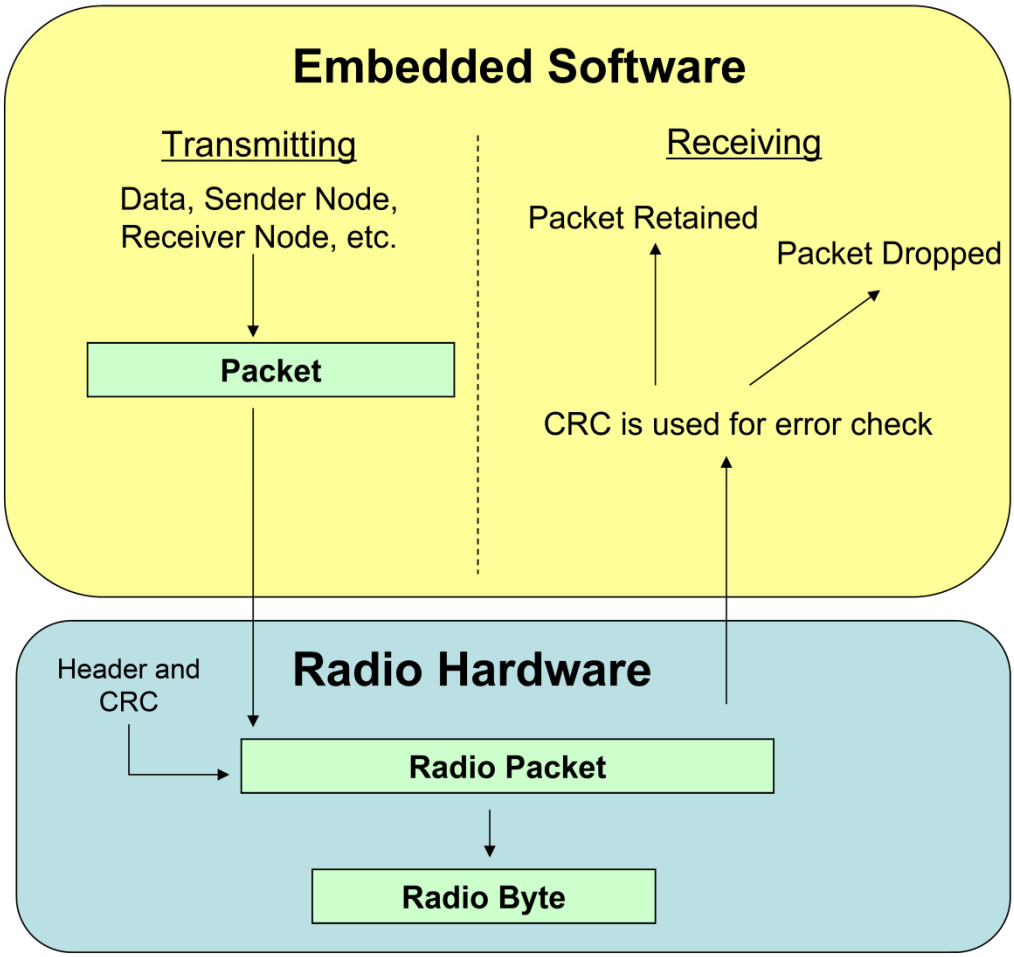

Figure 2.3: Framework for wireless communication.

QUANTITATIVE ANTENNA CHARACTERIZATION

In contrast to traditional wired monitoring systems, communication characteristics must be considered to determine sensor placement and resource consumption. Three items of primary interest are antenna type and orientation, communication range, and the influence of the sensor network environment. In this section, all three issues are examined experimentally for the Imote2.

3.1 Radiation Pattern Characteristics

While the hardware data sheets provide ideal performance characteristics, the as-built system requires careful evaluation to assess its actual performance. Anechoic chamber tests were conducted in the anechoic chamber in the Electromagnetics Laboratory at the University of Illinois campus to determine the radiation pattern of the as-built sensor and to gain a better understanding of the antenna performance. Three configurations were considered: (1) onboard antenna, (2) external antenna, and (3) external antenna, in conjunction with an environmentally hardened enclosure pictured in Fig. 3.1.

The environmentally hardened enclosure is designed to protect the sensor nodes from the weather and to facilitate attachment to the structure to be monitored. The enclosure is a PVC non-metallic junction box that carries a NEMA 6P rating, which protects against rain and water submersion. Furthermore, the PVC does not significantly impact radio transmission.

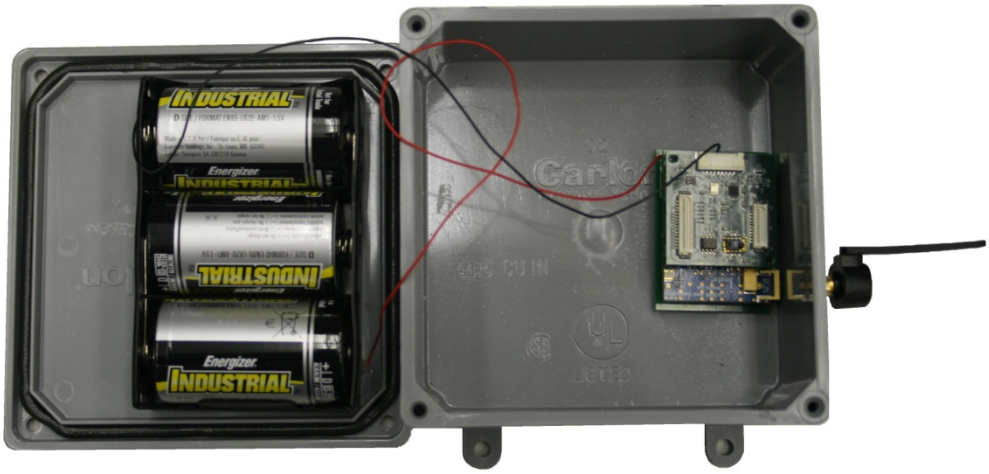

Figure 3.1: Imote2 in an Environmentally Hardened Enclosure.

Power radiated by an antenna varies as a function of the directional coordinates, and decreases as $1/d^2$ with increasing radial distance, d, from the antenna, in the far field. Radiation patterns are used to plot the variation in power as a function of angular position. For example, the radiation pattern for an isotropic antenna would be a sphere. While a complete description of the antenna pattern requires a three-dimensional plot, two-

dimensional polar plots are commonly used to convey the most important information, especially if the antenna radiation has a symmetric radiation pattern.

The polarization of an antenna is the direction of the electric field vector of the radiated wave and is dictated by geometry. The anechoic chamber uses a linearly polarized standard gain horn to measure the electric field transmitted by the antenna. The antennas being considering are supposed to be linearly polarized, which ideally means that the electric field is aligned in only one direction. However, antennas never radiate pure linearly polarized fields. Hence, fields are generally measured for two perpendicular orientations of the horn to characterize the complete field (Chang 2002). The electric field component in the desired orientation is referred to as the *co-polarized* field and any field in the perpendicular (undesired) direction is referred to as the *cross-polarized* field. Generally antennas with high polarization purity are desired, i.e., the co-polarized fields are considerably stronger than the cross-polarized fields. Co-polarized fields transfer the maximum signal whereas mismatched, or cross-polarized, fields typically transfer the least signal.

Testing Protocol

For the first two configurations, the antennas were run and powered by the Imote2 and its corresponding battery board to assess the as-built performance. The Imote2, powered by three AAA batteries, was mounted in a plastic support. As shown in Fig. 3.2 and Fig. 3.3, the same orientation was used for both the internal and external antenna configurations. Using the *ContinuousSend* test application (ISHMP 2008), dummy packets were sent continuously, while transmission and power measurements were taken at 10 degree intervals with an Agilent E4440A spectrum analyzer. The distance between the Imote2 and the measuring horn was 5.5 m. Co-polarized and cross-polarized field measurements were determined in the azimuthal plane (the plane of the table) and used to calculate power levels; elevation plane measurements (the plane perpendicular to the table, including the direction of measurement) were taken as well.

In the third configuration, the Imote2 with the external antenna was mounted in the environmentally hardened enclosure and tested to assess the impact of the enclosure on antenna performance. As in the previous tests, power measurements were taken at 10 degree intervals with the Agilent E4440A spectrum analyzer.

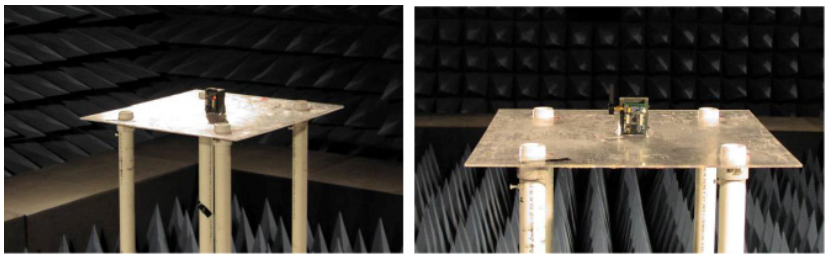

Figure 3.2: Onboard (left) and external (right) antenna set-up in anechoic chamber.

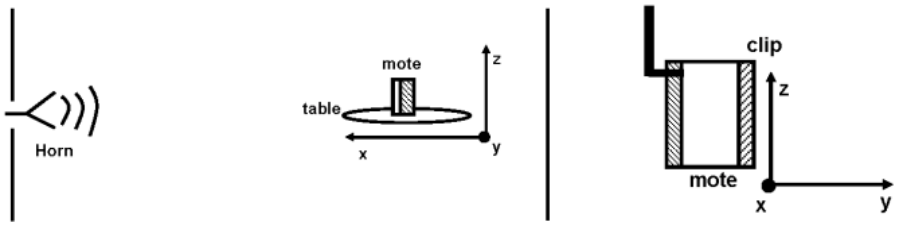

Figure 3.3: Anechoic chamber test set-up (left) and close-up of mote and antenna orientation at 0° (right).

Results

The power patterns for the co-polarized and cross-polarized electric fields of the antenna determined from the anechoic chamber tests are given in Fig. 3.4 and Fig. 3.5. The solid and dashed curves represent the onboard antenna and external antenna results, respectively.

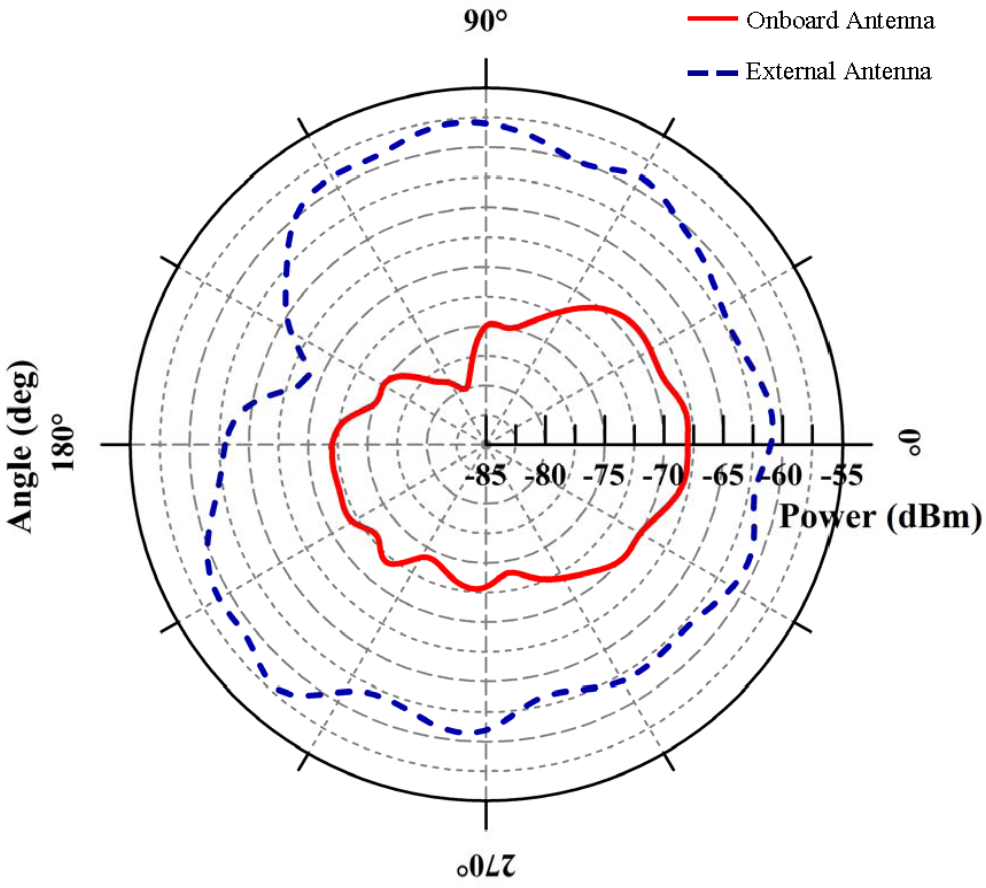

Figure 3.4: Co-polarization plots of onboard and external antennas.

The onboard antenna demonstrates a moderately isotropic pattern, with received power being ~ -70 dBm for both polarizations, in both the azimuthal and elevation planes. We see a slight preference for the 0° direction (where the front of the board faces the horn, as pictured in Fig. 3.3). Thus, this antenna has no ideal orientation for

communication. However, orienting two sensors with their antennas having identical orientations will provide better communication. For slightly improved performance, placing the sensors along the 0° direction (parallel and facing one another) will provide the best communication range if the onboard antenna is used, as the highest directivity is achieved.

The external antenna exhibits more dipole-like antenna characteristics. In the azimuthal plane (with the dipole axis perpendicular to the table), the co-polarized fields show fairly uniform power, which is about 10 dB above the average cross-polarization power. In the elevation plane patterns (not included here), the expected dipole-like pattern was seen. The performance may be further improved by orienting the antenna so that it is parallel with the board, which radiates as well.

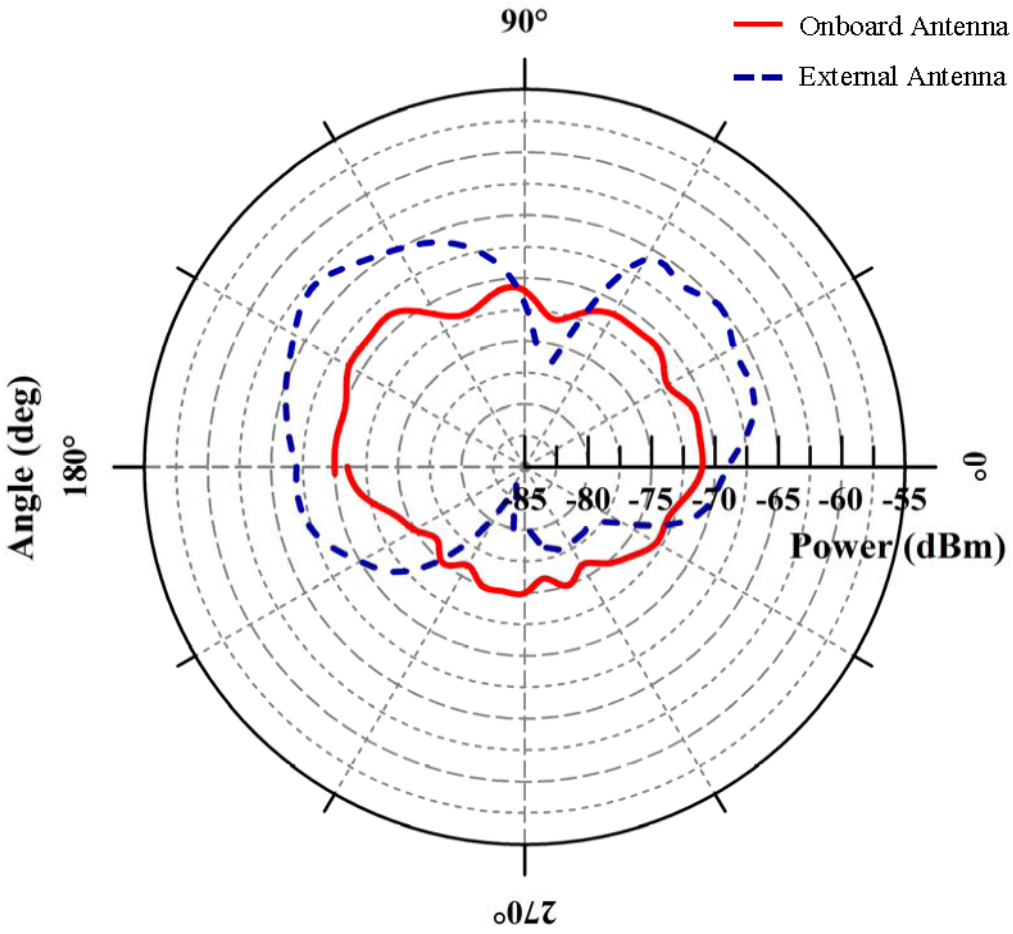

Figure 3.5: Cross-polarization plots of onboard and external antennas.

The external antenna and the enclosure resulted in the same pattern as the external antenna on its own; however, the radiated power with the enclosure was about 5 dB higher than that without the enclosure. This is most likely due to improvements in the antenna impedance match caused by the presence of the enclosure. The similarity in pattern characteristics demonstrates that the enclosure does not negatively impact the external antenna's performance – indeed, its presence actually improves the antenna's ability to transmit and receive signals.

In their ideal orientations, the external antenna power is about 7 dB better than the onboard antenna, which corresponds to about five times more power in linear units. Since power decays as a function of $1/d^2$ for large distances, where d is distance, use of the external antenna should result in communication ranges that are at least double those found when employing the onboard antenna.

3.2 Ideal Communication Range

The ideal communication range of the as-built Imote2 is determined in the absence of environmental factors that reduce the quality of the transmission signal. While the ideal communication ranges are not expected to be achieved in an implemented wireless sensor network, they do provide a baseline for comparison of various power, frequency, and antenna configurations.

Testing Protocol

To assess the packet loss associated with single-hop communication, the testing protocol performed loopback tests for various (1) power levels, (2) communication channels, (3) sensor and antenna orientations, and (4) environmental factors. A loopback test consists of sending a set number of packets from the sender node to a remote node. The remote node records the number of packets it receives and then sends this information, along with the received packets, back to the sender. Finally, the sender records the number of packets it receives from the remote node. The final results of the loopback test are (1) the number and percentage of packets that made it to the remote node and (2) the number and percentage of packets that made the complete round-trip back to the fixed sender. For each set of test parameters, the loopback test was repeated at least five times to obtain an average packet reception rate. The distance between the sender and remote node was slowly incremented until failure occurred. All tests were conducted on the same day and in succession. Any temporal effects were considered minimal, as tests run using "cold" motes and "hot" motes, sensor nodes that had been used for a significant period of time, resulted in little variation in response.

The loopback tests were run on the Imote2 using the *TestRadio* test application (ISHMP 2008). Fig. 3.6 shows a flow chart of how *TestRadio* is used to perform the loopback tests. At the start of the test, the user specifies the transmission channel, transmission power, the ID of the remote node(s) (up to 10 remote nodes may be tested at one time) and the number of packets to be sent. The power levels correspond to an output power and current consumption, which are given in Table 2.1. Note that all of the command packets used to perform the tests are sent using a reliable communication protocol, which consists of acknowledging receipt and resending of command packets to ensure delivery, while the packets sent to test the communication performance are sent only once. This approach ensures that the command packets are received and that poor communication performance will not result in premature termination of the test application. When the communication distance becomes too great, the command packets being sent reliably will not reach their intended target and the test times out, resulting in a failure.

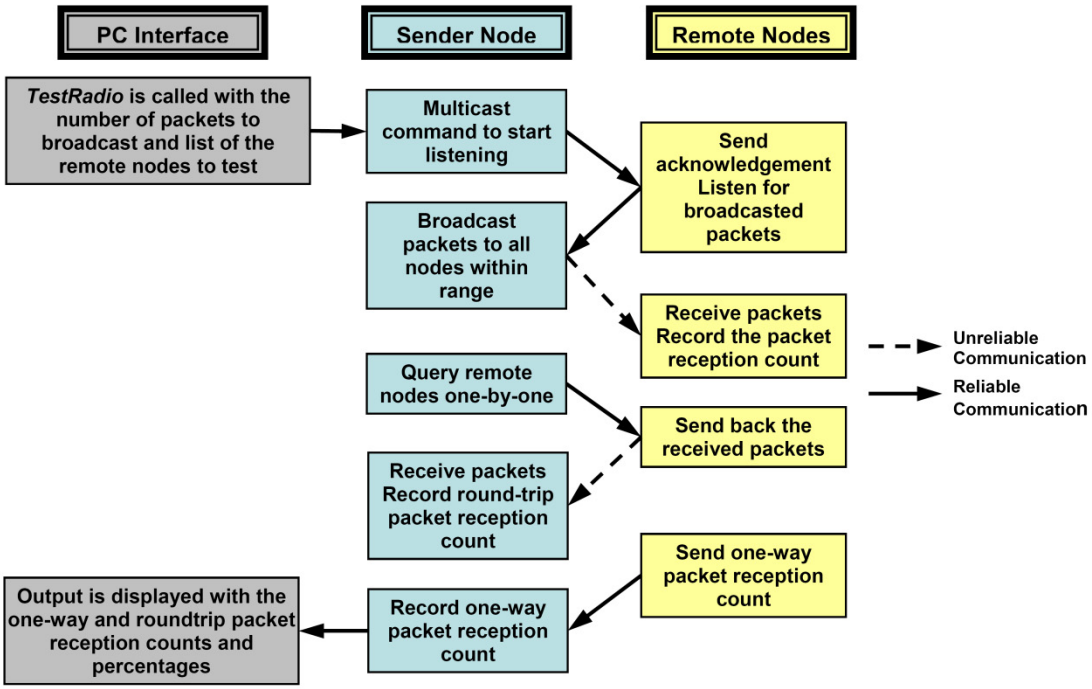

Figure 3.6: Loopback test implementation with the TestRadio application.

Beyond the testing program, the antenna orientation and environmental setting can be adjusted as desired. Two variables were kept constant throughout all tests: the sensor nodes were kept at a constant height of 1.22 meters, or 4 feet, off the ground, and 1000 packets were sent between nodes.

The quantitative measurement of packet delivery performance used in these tests was the packet reception rate. This value refers to the number of packets that were received out of the total number of packets sent. The complement measurement of packet reception rate is packet loss, which is the number of packets lost out of the total number of packets sent. While there is usually a correlation between packet reception rate and link quality indicators, such as RSSI, these indicators in individual radios vary greatly from one another in their sensitivities and accuracies. Thus, packet reception rate provides a more quantitative and repeatable metric over multiple radios.

For the ideal communication range tests, the influence of environmental factors was kept to a minimum. The tests were conducted outdoors with an unobstructed line-of-sight (LOS) between sensor nodes with no other 2.4 GHz wireless networks present. Fig. 3.7 illustrates the testing environment. Based on the radiation patterns determined from the anechoic chamber tests, the sensor nodes were oriented vertically and parallel to one another for both the onboard and external antenna communication range tests. The external antennas were vertical and parallel to one another and the board. In this set of experiments, two remote sensor nodes were used with one base node to test for variation in performance among sensor nodes. The two remote sensor nodes were placed 6 feet apart to reduce the possibility of mutual interference.

Figure 3.7: Outdoor Testing Environment.

Results

The results for the outdoor loopback tests using transmission power 31 with the onboard and external antenna are given in Fig. 3.8. The largest distance given is the distance just before the tests could no longer be completed and corresponds to the maximum communication range of that configuration.

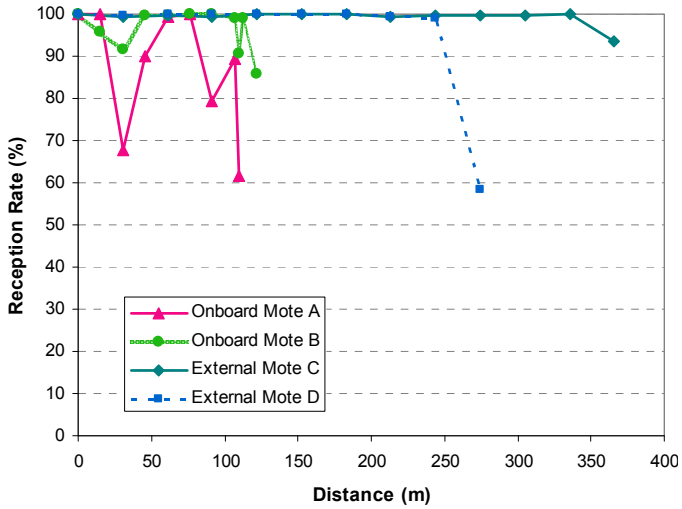

Figure 3.8: Onboard and external antenna performance at power level 31.

The external antenna performance is significantly better than the onboard antenna, as was indicated by the anechoic chamber tests. The external antenna outperformed the onboard antenna in both distance and consistency. At the same power level, the external antenna reached 366 meters, or 1200 feet, with a 92% packet reception rate, which is three times the distance of the onboard antenna. Furthermore, the onboard antenna exhibited somewhat inconsistent communication ranges as the reception rate fluctuates significantly over short distances while the external antenna exhibited more consistent behavior, yielding a reception rate of nearly 100% prior to the final drop-off, which is typical of digital data transmission.

For both antenna configurations and all power levels, a visible variation in the performance is seen for different remote sensor nodes. In these tests, one node consistently underperforms the other in communication range; however, they exhibit similar reception rate behavior. This variation in performance can be attributed to the variability in off-the-shelf components used to manufacture the sensor node. Based on the shorter of the two communication ranges, an estimated usable communication range for optimal antenna orientation is established and given in Table 3.1. When comparing the onboard to the external antenna range at power 31, the ratio of usable communication range is about 2.3. This matches the anechoic chamber results, as a 7 dB performance differential corresponds to about 2.25 times more distance. Due to the variation of components and the influence of multi-path effects, which are impossible to completely eliminate, the anechoic tests correspond well with the experimental results.

Table 3.1: Usable communication range for optimal orientation.

Antenna Configuration	**Usable Communication Range (m)**
Onboard *Power 31*	107
External *Power 5*	122
External *Power 10*	152
External *Power 31*	243

3.3 Influence of Environmental Factors

While the ideal communication range tests indicate the optimal performance of the Imote2 communication hardware, these conditions will seldom exist for sensor deployments on civil infrastructure. Thus, the influence of common building environments and materials will be explored in this section. In particular, the impact of other networks, steel and concrete structures, and concrete masonry unit (CMU) infill will be addressed. Because we are more interested in the ultimate influence of the built environment, the quantitative measure of the impact will be reported as the reduction in the baseline reception rate that was observed in the corresponding testing environment without the obstacle being considered. Based on the radiation patterns determined from the anechoic chamber tests the sensor nodes in each of the following tests were oriented parallel to one another and the external antennas were vertical and parallel to one another and the board. In addition, the sensors were mounted vertically on wooden poles 1.22 meters, or 4 feet, above the ground so that the experimenters were not in proximity to the sensors and their presence did not distort the measurements. Table 3.2 at the end of the section combines the results from all tests.

Wireless Networks

Wireless sensors using the IEEE 802.15.4 (Zigbee) protocol, which is commonly used for low-power devices, operate over the same 2.4 GHz band as wireless LAN (WLAN) devices using IEEE 802.11b,g protocols (Wi-Fi). Fig. 3. 9 illustrates this wireless channel overlap. Given this situation, each device can experience interference from the transmissions on the other network (Shin et al. 2007), degrading performance and leading to packet loss. IEEE 802.15.4 standards recommend using the clear channels where the energy of the Wi-Fi network is typically lower (Hubler 2005); however, if many IEEE 802.15.4 devices are operating in the area, using the clear channels may not ensure that interference is avoided (Shin et al. 2007).

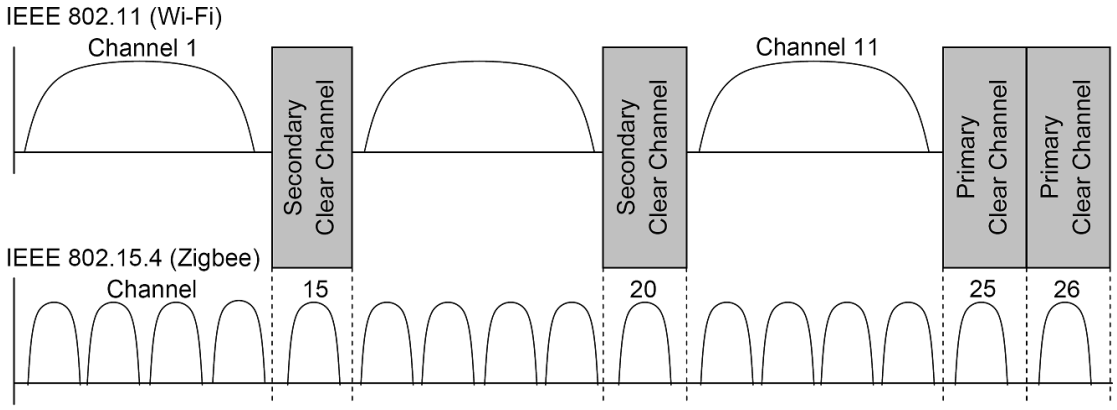

Figure 3.9: Wireless channel overlap for 802.11 network and 802.15.4 spectrum.

Given the possible interference of wireless networks with sensor communication, the impact of the WLAN on communication reliability was evaluated with loopback tests in the Newmark Civil Engineering Laboratory on the University of Illinois Urbana-Champaign campus. The tests were conducted in an open portion of the crane bay. The wireless network in the building operates on channel 11, which corresponds to channels 21 through 24 in the 802.15.4 spectrum.

Two sets of tests were conducted with the sensor nodes placed 7.6 meters, or 25 feet, and operating at full radio power (Power Level 31). First, loopback tests were conducted on 802.15.4 channel 11, which falls within 802.11b channel 1, and therefore outside of the operating frequency of the Wi-Fi network in the building; this configuration was considered as the baseline. Next, loopback tests were conducted within the wireless network channel (802.11 channel 11) operating in the building. Screenshots (Fig. 3.10) produced using a WiSpy v.1 by MetaGeek spectrum analyzer illustrate the two test configurations. WiSpy is a 2.4GHz spectrum analyzer that measures the amplitude of signals over the 802.11b frequency bandwidth. The plots show frequency (or channel) vs. transmission power over time. The numbers along the x-axis correspond to 802.11b channels and time is reflected on the z-axis into the page, where the current reading is at the intersection of the x and z-axis.

Communication within the wireless channel resulted in a 15% reduction in baseline reception rate, in contrast to communication outside the wireless channel, which was unaffected. While the decrease is not drastic, it is significant and has the potential to

affect the overall sensor network performance and power consumption. With some knowledge of other networks in the proximity operating in the 2.4 GHz bandwidth, this interference can be avoided through careful operating channel selection.

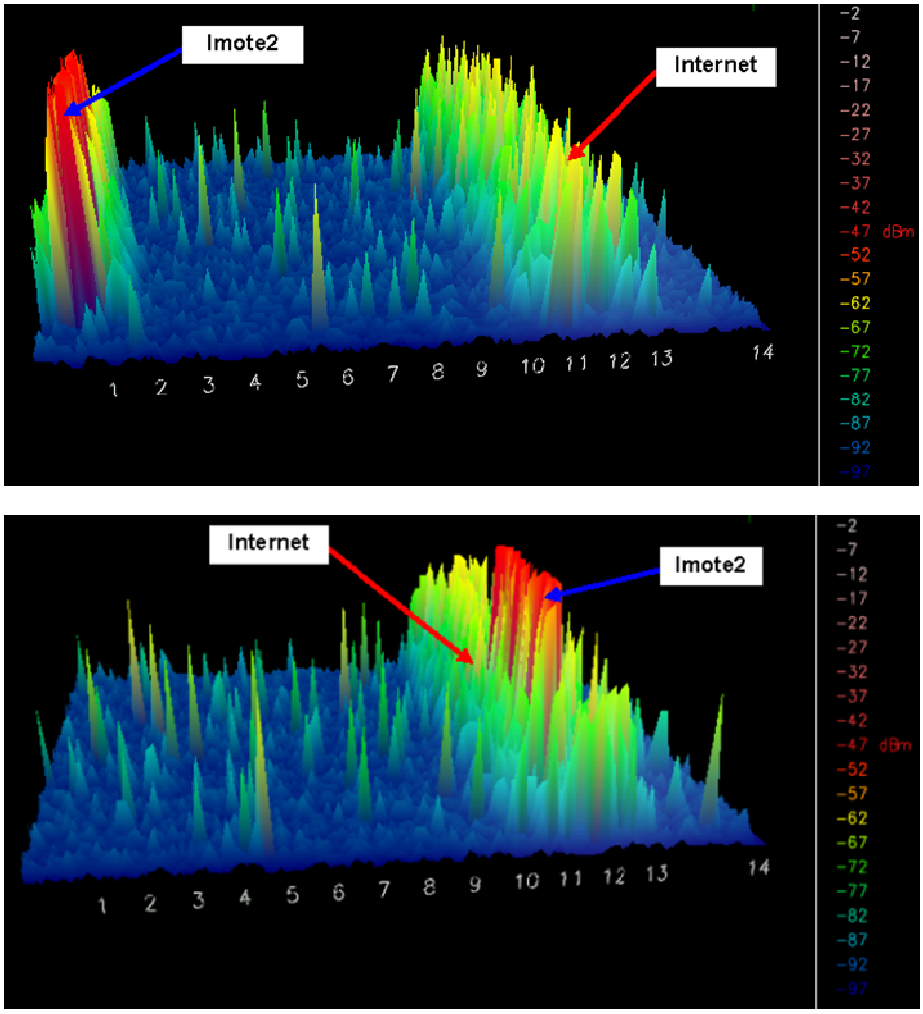

Figure 3.10: Communication outside of wireless internet channel (top) and communication within wireless network channel (bottom).

Steel Structures

The first of the building material types considered is steel. Given that one would not be able to transmit directly through a steel member, a steel building with poured concrete floors and typical finishing was used as a representative test of the expected signal attenuation to occur in a steel frame structure. A set of loopback tests were conducted in the Seibel Center for Computer Science on the University of Illinois Urbana-Champaign campus using two sensor nodes with external antennas as pictured in Fig. 3.11.

The tests consisted of two parts. In the first, the sensor nodes were located in a multi-story atrium in the center of the structure. One sensor node was placed on the upper level while the second sensor node was located a line-of-sight distance of 5.8 meters, or 19 feet, away. This configuration is considered as the baseline. In the second test, the sensor nodes were moved into the structure so the floor system was in-between and they were no

longer line-of-sight but still 5.8 meters apart as before. Two separate power levels were tested: power level 20 and power level 31. Power level 20 corresponded to the lowest transmission power required for a 100% reception rate in the atrium. In both cases, the steel structure resulted in approximately a 10% reduction in the baseline reception rate.

Figure 3.11: Representative Steel Structure and Detail of Floor System.

Reinforced Concrete Structure

Reinforced concrete structures typically consist of both reinforced concrete framing and floor systems. A parking garage on the University of Illinois campus was chosen as an extreme test situation for the attenuation due to reinforced concrete, since parking garages are usually heavily reinforced. A set of loopback tests was conducted using two sensor nodes and external antennas.

Two types of tests were conducted. In the first, line-of-sight tests were conducted on the upper floor of the parking garage. One sensor node was placed on the upper level of the garage on an overhang above the ramp below while the second, fixed, sensor node was placed a LOS distance of 5.8 meters, or 19 feet, away on the ramp to the lower story as shown in Fig. 3.12. This configuration was considered as the baseline. In the second test, the garage structure was located between the two sensor nodes and they were no longer line-of-sight. The remote sensor node was moved down exactly two stories such that remote node was ultimately one story below the fixed node and the concrete garage was in-between the nodes. Thus, the sensor nodes were still 19 feet apart but no longer line of sight. Three power levels were tested: power levels 4, 5, and 10. Power level 4 was the highest power setting where packet loss was observed, due to the garage.

Figure 3.12: Reinforced Concrete Testing Environment.

Overall, a negligible decrease in the reception rate was found due to the concrete structure as compared to the baseline configuration. Even at power level 4, the decrease in reception rate was only about 1%, while at higher power levels, no observed change in reception rate was observed. While losses in an R/C structure are expected, it is difficult to ascertain or anticipate the effects of the reinforcement since it depends on the configuration and spacing of the reinforcement and the relationship between this spacing/configuration and the operating wavelength. In fact, in some cases, the presence of the reinforcement along a corridor may actually encourage propagation along the corridor due to the effective guiding of the transmitted electromagnetic wave.

Concrete Masonry Infill

Concrete masonry unit (CMU) infill walls are common in many civil engineering structures. A set of loopback tests were conducted in a classroom area in the Newmark Civil Engineering Building on the University of Illinois campus to evaluate the degree of attenuation. The testing environment is pictured in Fig. 3.13.

Again, the tests consisted of two parts. In the first test, one sensor node was located inside a classroom 6.1 meters, or 20 feet, line-of-sight through the doorway from the second sensor node in the hallway; this configuration was considered as the baseline. In the second test, the sensor nodes were moved east in the classroom and hallway respectively until the CMU wall was in-between and they were no longer line-of-sight, but still 6.1 meters apart. The tests were conducted at transmission power 10. Power level 10 was the lowest power level at which a 100% reception rate was achieved in the line-of-sight baseline configuration.

The CMU infill resulted in a negligible reduction in the reception rate. This result is promising for other types of partitions that might be used in civil engineering structures such as gypsum board.

Figure 3.13: CMU Test Environment.

Table 3.2: Overall attenuation results of built environment elements.

Built Environment Element	Reduction in Reception Rate (%)
Wireless Network	15
Steel Structure	10
Reinforced Concrete	~ 0
CMU Infill	~ 0

BRIDGE IMPLEMENTATION

Wireless communication tests were conducted on a bridge in Mahomet, Illinois, for which a full-scale implementation of a smart sensor network is underway. The bridge, pictured in Fig. 4.1, is a turn-of-the-century steel truss bridge now used for pedestrian traffic. The tests performed on this bridge determined the antenna power required for at least 95% reception rate between girders.

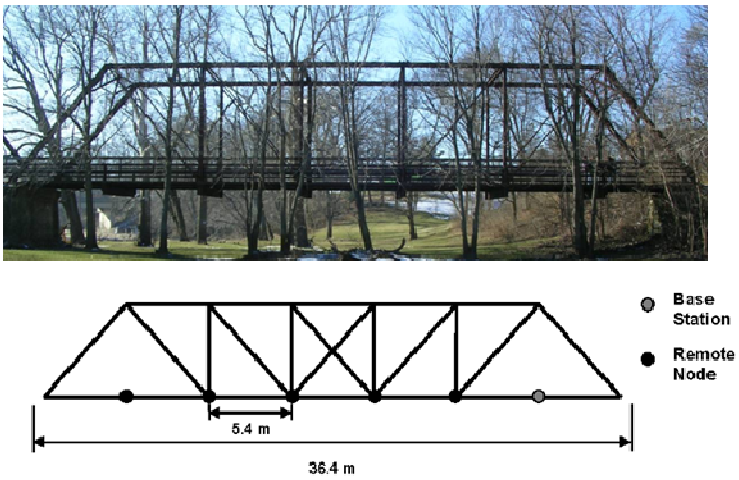

Figure 4.1: Steel truss bridge in Mahomet, Illinois (top) and testing layout and dimensions (bottom).

Test Protocol

Given a proposed sensor layout for monitoring the bridge, the bridge geometry, and the radiation pattern tests reported in the section outlining the anechoic chamber test results, the following test protocol was developed. The sensor layout assumes that a majority of the sensors will be located at the nodes of the truss along the face of bridge and a couple sensors will be located across the deck of the bridge to capture torsional behavior. The fixed node was placed underneath the bridge on the girder closest to the north support (on the right in Fig. 4.1). The remote node was moved from girder to girder underneath the bridge. The sensor nodes were located in the environmentally hardened enclosure and two antenna configurations were considered: the external antenna aligned perpendicular to the plane of the bridge, which is optimal for communication along the face of the bridge, and parallel to the face of the bridge, which is considered poor for communication along the face of the bridge but optimal for communication across the deck of the bridge.

Results

Table 4.1 gives the power required to achieve at least 95% reception rate for both antenna orientations. Based on the ideal communication results previously reported, use of the external antenna at power level 5 should be sufficient to reach to the furthest girder with at least 95% reception rate; however, Table 4.1 indicates that a power of 10 is needed in

the optimal orientation, while a power of 15 is required for the suboptimal orientation. Therefore, the steel structure had a considerable impact on the antenna performance. These results highlight the need to consider the built environment and conduct on-sight testing prior to network implementation. For example, the higher power level required at 15.6 m is likely due to multi-path losses. The signal would reflect off the river bed and possibly propagate along the bridge. Although multi-path effects can be beneficial, this is an example of detrimental multi-path effects. Furthermore, in-situ tests could be used to optimize network communication protocols by selecting the optimal power level for a specific type of communication, i.e., single-hop or multi-hop.

Table 4.1: Power level required for 95% reception rate, Mahomet, Illinois.

Distance to Girder (m)	**Power Level Required**	
	Optimal Orientation	*Suboptimal Orientation*
5.2	5	5
10.4	5	5
15.6	15	10
20.8	10	15
26	10	15

CONCLUSION

This report examines the wireless performance of the Imote2 smart sensing platform. Through anechoic chamber tests, communication range tests, and tests in common sensor network environments, a quantitative characterization of the wireless communication performance of the Imote2 platform with both onboard and external antennas was determined. Finally, these results were applied to a full-scale bridge implementation.

Anechoic chamber testing revealed the optimal antenna orientation for both the onboard and external antennas. Subsequent communication range testing using these optimal antenna configurations showed that the external antenna improves both the ideal transmission range and the communication reliability for all transmission power levels. However, inevitable environmental factors reduce achievable communication ranges even with the most effective antenna orientation. To assess this effect, additional communication range testing was conducted in the presence of common building materials. Of the building materials tested, steel proved to have the most significant effect on the achievable communication range as one would expect; sensor networks in the presence of steel structural members may require higher transmission power to realize adequate communication distances. While signal attenuation due to building materials is difficult to avoid, interference resulting from other wireless networks sharing the same frequency band can be avoided through careful transmission channel selection. For full-scale sensor network implementations, it is recommended to use external antennas with the optimal orientation. In-situ loopback testing may be done to determine the minimum required transmission power to achieve acceptable communication levels in the sensor network environment while managing network resources.

REFERENCES

Antenova. (2007a). *Antenova Mica 2.4 GHz SMD Antenna Product Specification*. Antenova.

Antenova. (2007b). *Antenova Titanis 2.4 GHz Swivel SMA Antenna Product Specification*. Antenova.

Buonadonna, P., Hill, J., and Culler, D. (2002). "Active Message Communication for Tiny Networked Sensors"< www.tinyos.net/papers/ammote.pdf> (Oct. 23, 2008).

Chang, K. (2002). *RF and Microwave Wireless Systems.* Wiley and Sons, New York.

Grimmer, M. and Suh, J. (2005). "Implementing Wireless Sensor Networks: Radio Communication Links and Compact/Internal Antennas" Version 1.0, Crossbow Technology Inc.

Hubler, T. (2005). "Worry-free Wireless Networks" *Networked Controls,* Penton Media.

Hyas, M. and Radha, H. (2008). "Measurement Based Analysis and Modeling of the Error Process in IEEE 802.15.4 LR-WPANs." *Proc., of the 27th IEEE Int. Conference on Computer Communications (INFOCOM'08),* Phoenix, Az., 1948-1956.

ISHMP (2008). *Illinois Structural Health Monitoring Project*. See software distribution at http://shm.cs.uiuc.edu/software.html.

Lee, K. and Chanson S. (2002). "Packet Loss Probability for Real-Time Wireless Communications" *IEEE Transactions on Vehicular Technology,* 51(6), 1569-1575.

Levis, P., Madden, S., Polastre, J., Szewczyk, R., Whitehouse, K., Woo, A., Gay, D., Hill, J., Welsh, M., Brewer, E., and Culler, D. (2005), TinyOS: An Operating System for Sensor Networks. Ambient Intelligence, Weber, W., Rabaey, J.M., Aarts, E., Eds. 115-148, Springer, Berlin, Heidelberg.

Lynch, J.P. and Loh, K. (2006). A summary review of wireless sensors and sensor networks for structural health monitoring. *Shock and Vibration*, 38(2), 91-128.

Nagayama, T. and Spencer Jr., B.F. (2007). "Structural Health Monitoring Using Smart Sensors" *Newmark Structural Engineering Laboratory (NSEL) Report Series,* No. 1, University of Illinois, Urbana, IL (http://hdl.handle.net/2142/3521).

Nagayama, T., Sim, S.-H., Miyamori, Y., and Spencer Jr., B.F. (2007). "Issues in Structural Health Monitoring Employing Smart Sensors." *Smart Structures and Systems*, 3(3), 299-320.

Pei, J.S., Kapoor, C., Graves-Abe, T.L., Sugeng, Y.P., and Lynch, J.P. (2007). "An Experimental Investigation of the Data Delivery Performance of a Wireless Sensing Unit Designed for Structural Health Monitoring" *Structural Control and Health Monitoring,* 15(4), 471-504.

Seidel, S. and Rappaport T. (1992). "914 MHz Path Loss Prediction Models for Indoor Wireless Communications in Multifloored Buildings" *IEEE Transactions on Antennas and Propagation,* 40(2), 207-217.

Shankar, P.M. (2002). *Introduction to Wireless Systems*. Wiley and Sons, New York.

Shin, S.Y., Park, S.P., and Kwon W.H. (2007). "Mutual interference analysis of IEEE 802.15.4 and IEEE 802.11b" *Computer Networks*, 51(12), 3338-3353.

Spencer Jr., B.F., Ruiz-Sandova, M.E., and Kurata, N. (2004). "Smart Sensing Technology: Opportunities and Challenges" *Structural Control and Health Monitoring*, 11(4), 349-368.

Spencer Jr., B. F., Nagayama, T., and Rice, J. A. (2008). "Decentralized structural health monitoring using smart sensors." *Proc., SPIE Smart Structures and Materials*, 6932, San Diego, CA.

Zhao, J. and Govindan, R. (2003). "Understanding Packet Delivery Performance In Dense Wireless Networks." *Proc., of the 1st Int. Conference on Embedded Network Systems*, ACM, Los Angeles, Ca., 1-13.

List of Recent NSEL Reports

No.	*Authors*	*Title*	*Date*
006	Carrion, J. and Spencer, B.F.	Model-based Strategies for Real-time Hybrid Testing	Dec. 2007
007	Kim, Y.S., Spencer, B.F., and Elnashai, A.S.	Seismic Loss Assessment and Mitigation for Critical Urban Infrastructure Systems	Jan. 2008
008	Gourley, B.C., Tort, C., Denavit, M.D., Schiller, P.H., and Hajjar, J.F.	A Synopsis of Studies of the Monotonic and Cyclic Behavior of Concrete-Filled Steel Tube Members, Connections, and Frames	April 2008
009	Xu, D. and Hjelmstad, K.D.	A New Node-to-node Approach to Contact/Impact Problems for Two Dimensional Elastic Solids Subject to Finite Deformation	May 2008
010	Zhu, J. and Popovics, J.S.	Non-contact NDT of Concrete Structures Using Air Coupled Sensors	May 2008
011	Gao, Y. and Spencer, B.F.	Structural Health Monitoring Strategies for Smart Sensor Networks	May 2008
012	Andrews, B., Fahnestock, L.A. and Song, J.	Performance-based Engineering Framework and Ductility Capacity Models for Buckling-Restrained Braces	July 2008
013	Pallarés, L. and Hajjar, J.F.	Headed Steel Stud Anchors in Composite Structures: Part I – Shear	April 2009
014	Pallarés, L. and Hajjar, J.F.	Headed Steel Stud Anchors in Composite Structures: Part II – Tension and Interaction	April 2009
015	Walsh, S. and Hajjar, J.F.	Data Processing of Laser Scans Towards Applications in Structural Engineering	June 2009
016	Reneckis, D. and LaFave, J.M.	Seismic Performance of Anchored Brick Veneer	Aug. 2009
017	Borello, D.J., Denavit, M.D., and Hajjar, J.F.	Behavior of Bolted Steel Slip-critical Connections with Fillers	Aug. 2009
018	Rice, J.A. and Spencer, B.F.	Flexible Smart Sensor Framework for Autonomous Full-scale Structural Health Monitoring	Aug. 2009
019	Sim, S.-H. and Spencer, B.F.	Decentralized Strategies for Monitoring Structures using Wireless Smart Sensor Networks	Nov. 2009
020	Kim, J. and LaFave, J.M.	Joint Shear Behavior of Reinforced Concrete Beam-Column Connections subjected to Seismic Lateral Loading	Nov. 2009
021	Linderman, L.E., Rice, J.A., Barot, S., Spencer, B.F., and Bernhard, J.T..	Characterization of Wireless Smart Sensor Performance	Feb. 2010